

# Thermoresponsive Polymeric Nanolenses Magnify the Thermal Sensitivity of Single Upconverting Nanoparticles

Dasheng Lu, Jorge Rubio Retama, Riccardo Marin, Manuel I. Marqués, Oscar G. Calderón, Sonia Melle, Patricia Haro-González,\* and Daniel Jaque\*


Lanthanide-based upconverting nanoparticles (UCNPs) are trustworthy workhorses in luminescent nanothermometry. The use of UCNPs-based nanothermometers has enabled the determination of the thermal properties of cell membranes and monitoring of in vivo thermal therapies in real time. However, UCNPs boast low thermal sensitivity and brightness, which, along with the difficulty in controlling individual UCNP remotely, make them less than ideal nanothermometers at the single-particle level. In this work, it is shown how these problems can be elegantly solved using a thermoresponsive polymeric coating. Upon decorating the surface of NaYF<sub>4</sub>:Er<sup>3+</sup>,Yb<sup>3+</sup> UCNPs with poly(*N*-isopropylacrylamide) (PNIPAM), a >10-fold enhancement in optical forces is observed, allowing stable trapping and manipulation of a single UCNP in the physiological temperature range (20–45 °C). This optical force improvement is accompanied by a significant enhancement of the thermal sensitivity— a maximum value of 8% °C<sup>-1</sup> at 32 °C induced by the collapse of PNIPAM. Numerical simulations reveal that the enhancement in thermal sensitivity mainly stems from the high-refractive-index polymeric coating that behaves as a nanolens of high numerical aperture. The results in this work demonstrate how UCNP nanothermometers can be further improved by an adequate surface decoration and open a new avenue toward highly sensitive single-particle nanothermometry.

## 1. Introduction

The growing demand for remote local temperature monitoring in applications like micro/nanoelectronics, integrated photonics, and biomedicine has stimulated the development of luminescence nanothermometry.<sup>[1]</sup> This more-than-a-decade-old technology harnesses the relationship between local temperature and optical properties of luminescent nanothermometers (LNThs) to achieve thermal sensing. Among the proposed LNThs are semiconductor nanocrystals, organic dyes, and luminescent polymers.<sup>[1a,b]</sup> However, lanthanide-based upconverting nanoparticles (UCNPs), with their ability to convert low-energy photons into higher-energy ones, are particularly attractive LNThs because of their biocompatibility, photostability, multicolor narrowband emissions, and tunable lifetime.<sup>[2]</sup> For example, Er<sup>3+</sup>,Yb<sup>3+</sup>-doped UCNPs are popular LNThs based on two thermally coupled energy levels of Er<sup>3+</sup> ion (<sup>2</sup>H<sub>11/2</sub> and <sup>4</sup>S<sub>3/2</sub>).<sup>[3]</sup> Small temperature changes cause

D. Lu, R. Marin, P. Haro-González, D. Jaque  
Nanomaterials for Bioimaging Group (NanoBIG)  
Departamento de Física de Materiales  
Facultad de Ciencias  
Universidad Autónoma de Madrid  
Madrid 28049, Spain  
E-mail: patricia.haro@uam.es; daniel.jaque@uam.es

D. Lu, M. I. Marqués, P. Haro-González  
Instituto Universitario de Ciencia de Materiales Nicolás Cabrera  
Facultad de Ciencias  
Universidad Autónoma de Madrid  
Madrid 28049, Spain

 The ORCID identification number(s) for the author(s) of this article can be found under <https://doi.org/10.1002/smll.202202452>.

© 2022 The Authors. Small published by Wiley-VCH GmbH. This is an open access article under the terms of the Creative Commons Attribution License, which permits use, distribution and reproduction in any medium, provided the original work is properly cited.

DOI: 10.1002/smll.202202452

D. Lu, J. R. Retama, R. Marin, D. Jaque  
Nanomaterials for Bioimaging Group (NanoBIG)  
Instituto Ramón y Cajal de Investigación Sanitaria  
IRYCIS  
Ctra. Colmenar km. 9.100, Madrid 28034, Spain

J. R. Retama  
Departamento de Química en Ciencias Farmacéuticas  
Facultad de Farmacia  
Plaza de Ramón y Cajal  
s/n  
Universidad Complutense de Madrid  
Madrid 28040, Spain

M. I. Marqués  
Departamento de Física de Materiales and IFIMAC  
Universidad Autónoma de Madrid  
Madrid 28049, Spain

O. G. Calderón, S. Melle  
Departamento de Óptica  
Facultad de Óptica y Optometría  
Universidad Complutense de Madrid  
Madrid 28037, Spain

relevant electron population redistribution and, hence, noticeable changes in the intensity ratio between the corresponding emission lines. Although such ratiometric thermal sensing is a reliable approach, the associated thermal sensitivities are generally around  $1\% \text{ } ^\circ\text{C}^{-1}$  at room temperature, leading to limited thermal resolutions.<sup>[16,4]</sup> Additionally, the acquisition of thermal images using UCNP usually requires the incorporation of large amounts of UCNP in the system.<sup>[5]</sup> Such massive incorporation of UCNP could have adverse effects and interference, particularly in biological systems, such as living cells or tissues.<sup>[6]</sup> As scanning probe microscopy matures,<sup>[7]</sup> scanning thermal imaging can be performed by precisely manipulating a single UCNP acting as a probe in 3D space. This strategy avoids the massive incorporation of UCNP but requires new strategies to improve their thermal sensitivity while allowing their remote manipulation.

In the context of sensing with single nanosensors, optical trapping (OT) is the prime choice as a versatile and reliable noncontact tool for the 3D manipulation of single particles.<sup>[8]</sup> OT of nanoparticles is based on optical forces originating from the interaction between the inhomogeneous electromagnetic field and the induced particle's polarization.<sup>[9]</sup> This interaction allows achieving thermal imaging by scanning a single particle in the three dimensions while recording its emission spectrum (if trapping radiation is partially absorbed by ytterbium ions within the UCNP). Upconversion-enabled 3D thermal sensing has been demonstrated with OT of microparticles.<sup>[8e,10]</sup> Yet, moving from the micro- to the nanoscale the 3D scanning capability of OT becomes limited.<sup>[11]</sup> Indeed, the optical trapping force acting on sub-100 nm UCNP is typically below  $0.01 \text{ pN}$ .<sup>[11a]</sup> This low optical force is insufficient to overcome the drag force generated by the surrounding medium (usually water). Furthermore, for UCNP, the trap potential is comparable to the thermal energy.<sup>[12]</sup> The result is that a slight increment of temperature can cause the release of the UCNP from the trap. This effect precludes thermal scanning and, hence, thermal imaging above room temperature. Thus, the optical force should be magnified for reliably scanning a single UCNP above room temperature.

Surface decoration of UCNP is an effective method to enhance the optical force of sub-100 nm UCNP while improving their multifunctionality.<sup>[13]</sup> By precise control of the coating layer thickness and chemical nature, coated colloids can be prepared with different exposed functional groups and featuring better colloidal stability, narrower size dispersion, and superior biocompatibility.<sup>[14]</sup> Furthermore, changes in surface functional groups are accompanied by variations in the amount and distribution of charges on the surface of UCNP dispersed in liquid media, which are directly correlated with their  $\zeta$ -potential. Importantly, it has been shown that optical forces acting on UCNP can be tailored as a function of the  $\zeta$ -potential.<sup>[9b,13a]</sup> However, one avenue that remains unexplored in this context is the use of thermoresponsive polymers to simultaneously control the surface charge of the UCNP and profit from the temperature-dependent properties of the coating. Indeed, surface modification with a thermoresponsive polymer was shown to be a powerful strategy to elicit temperature-dependent spectral changes in core-shell nanoparticles as an ensemble.<sup>[15]</sup> It is therefore envisaged that similar drastic

modulation of the spectroscopic properties would arise in single UCNP during optical trapping.

In this work, a thermoresponsive polymer (poly(*N*-isopropylacrylamide, PNIPAM),<sup>[16]</sup> was coated on the surface of a 30 nm  $\text{NaYF}_4:\text{Er}^{3+}, \text{Yb}^{3+}$ , UCNP to obtain a structure (UCNP@PNIPAM). The optical forces acting on a single UCNP@PNIPAM have been measured in the 20–45 °C temperature range and compared to those acting on bare UCNP. The improvement in optical force caused by the PNIPAM coating has been explained in terms of changes in surface charge, effective refractive index, and size of the UCNP@PNIPAM structures. The emitted intensity generated by an optically trapped UCNP@PNIPAM has been also systematically measured as a function of temperature revealing an anomalous behavior that leads to superior thermal sensitivity. Numerical simulations have been conducted to understand the sharp temperature-induced increment of the collected signal that occurs in correspondence to the collapse temperature of the PNIPAM coating, which acts as a nanolens with a high numerical aperture.

## 2. Results and Discussion

### 2.1. Synthesis and Characterization of UCNP@PNIPAM Structures

The UCNP@PNIPAM structures were prepared following a modified, reported thermal decomposition method,<sup>[17]</sup> followed by surface modification with the thermoresponsive polymer (Figure 1a). A detailed description of the whole process can be found in Section S1 of the Supporting Information. The UCNP have an average diameter of  $(30 \pm 2) \text{ nm}$  and the typical hexagonal disk-shape of  $\beta\text{-NaYF}_4:\text{Er}^{3+}, \text{Yb}^{3+}$  (Figure 1b). Around each UCNP core, a PNIPAM shell of 100 nm in thickness (as obtained from transmission electron microscope (TEM) images) was homogeneously grown (Figure 1c). The resulting UCNP@PNIPAM units have a uniform size of  $(230 \pm 20) \text{ nm}$  in diameter. Different magnification images of a single UCNP@PNIPAM structure are shown in Figure 1d,e.

The hybrid UCNP@PNIPAM structures were dispersed in water, where the particles are positively charged ( $\zeta$ -potential +16.9 mV, Figure 1f). The PNIPAM coating swells in water at room temperature, inducing the ordering of water molecules around the amide group by means of hydrogen bonding<sup>[18]</sup> (Figure 1g). When the temperature is above the volume phase transition temperature (VPTT  $\approx 32 \text{ } ^\circ\text{C}$ ), molecular agitation disrupts the hydrogen bonds and leads to a breakdown of the local water structure around the PNIPAM chains (Figure 1g). This process known as volume phase transition (VPT) increases the hydrophobicity of the polymer network and triggers hydrophobic attractions among isopropyl groups, with the consequent “squeezing-out” of water molecules from the polymer structure. The result is a transition from a swollen state to a collapsed state, yielding a reduction of the hydrodynamic diameter as well as an increment of the refractive index of the PNIPAM coating.<sup>[19]</sup> This VPT was studied by measuring the hydrodynamic diameter of the nanoparticles as a function of the temperature using dynamic light scattering (DLS, Figure 1h). Note that the hydrodynamic diameter reported in

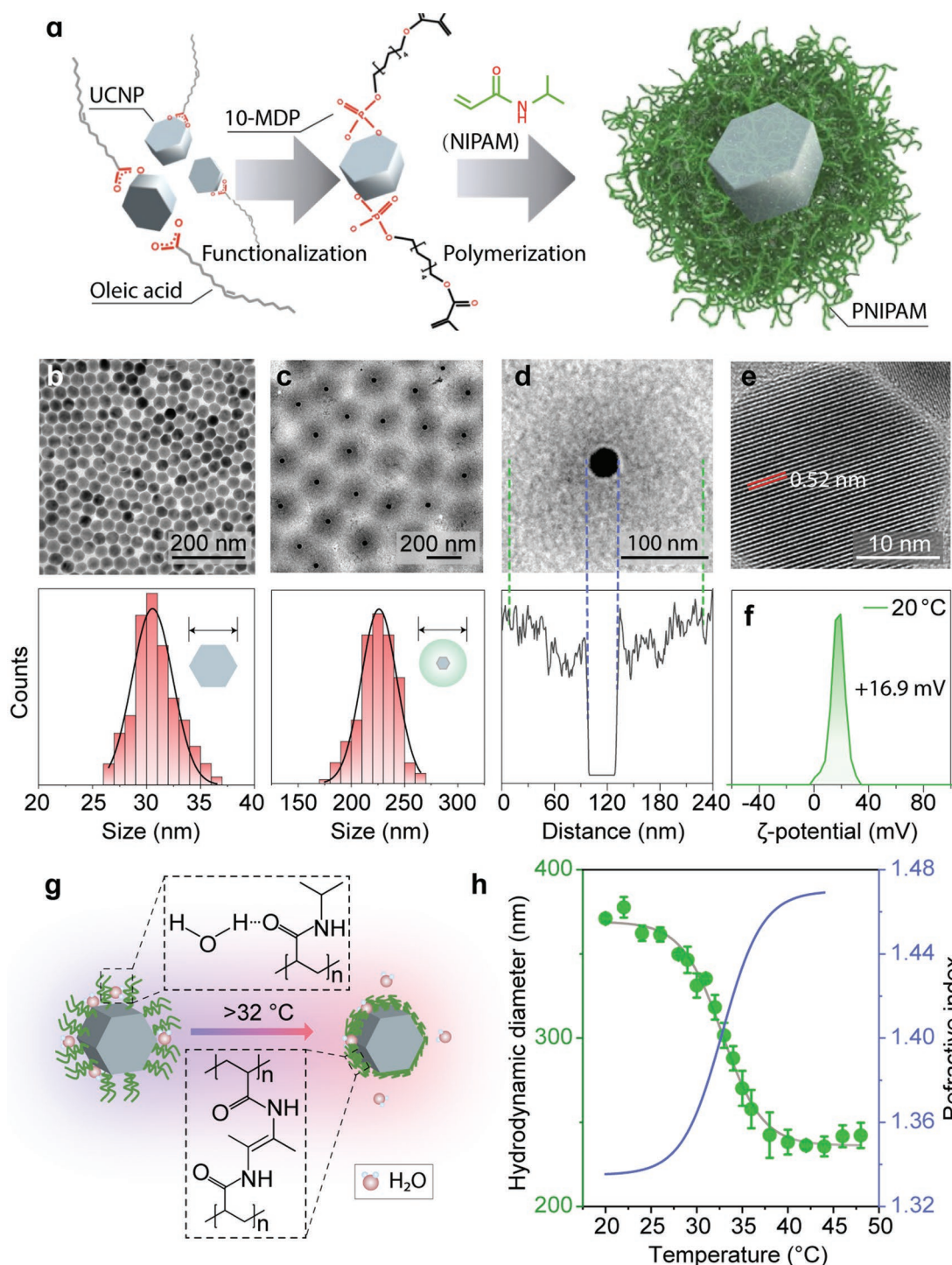


**Figure 1.** a) Schematic illustration of the modification of UCNP with PNIPAM. b) TEM image of bare UCNPs. The figure right below shows the corresponding histogram of size distribution. c) TEM image of UCNP@PNIPAM structures. The figure right below shows the corresponding histogram of size distribution. d,e) TEM images of a single UCNP@PNIPAM with different magnifications. Intensity profile as obtained from (d) indicating the location and size of core UCNP and entirety. f)  $\zeta$ -potential of UCNP@PNIPAM structures dispersion at 20 °C. g) Schematic of the volume phase transition of UCNP@PNIPAM structures dispersed in water. h) The hydrodynamic diameter of UCNP@PNIPAMs structures dispersion characterized by dynamic light scattering (DLS) measurement (three times measurements were performed at each temperature, the gray solid curve is the sigmoidal fitting curve) and calculated refractive index curve of PNIPAM shell (blue solid line). The refractive index of PNIPAM in the swollen and collapsed state was considered 1.33<sup>[21]</sup> (matching the one of water) and 1.47<sup>[22]</sup> (bulk PNIPAM refractive index), respectively. The change of the refractive index with temperature was simulated as a sigmoidal function using the parameters extracted from the fit of the volume phase transition.

Figure 1h was given by Z-average values, which are intensity weighted and can be obtained by fitting corresponding correlograms. The respective correlograms and intensity-weighted size distribution curves were added in Section S2 of the Supporting Information. DLS experiments reveal a narrow size distribution being for any temperature below 15%, thus indicating the growth of a homogenous PNIPAM coating on the surface of UCNPs. Between 20 and 30 °C, PNIPAM is in a swollen state, hence the UCNP@PNIPAM structures exhibit a mean hydrodynamic diameter close to 370 nm. When the temperature is close to the VPTT, the polymer chain begins to collapse expelling the molecules of water from the matrix. The hydrodynamic diameter consequently shrinks down to a minimum of  $\approx 240$  nm at 37 °C. Further increment of the temperature does not produce any relevant variation of the hydrodynamic diameter. This behavior can be described by a four-parameter sigmoidal function<sup>[20]</sup>

$$D(T) = D_{\min} + \frac{D_{\max} - D_{\min}}{1 + \exp\left(\frac{T - T_{\text{tran}}}{\tau}\right)} \quad (1)$$

where  $D(T)$  is the diameter of the UCNP@PNIPAM structures at temperature  $T$ ,  $D_{\min}$  and  $D_{\max}$  are the minimum and maximum diameters (i.e., in the fully collapsed and swollen states), respectively,  $T_{\text{tran}}$  is the midpoint transition temperature (the inflection point of the curve, which can be identified as the VPTT), and  $\tau$  is the half-width of the transition. The quality of the nonlinear regression is excellent ( $R^2 = 0.992$ ), and the values of the parameters resulting from the fitting procedure are reported in Table 1. The VPT leads not only to a reduction

**Table 1.** Fitting parameters of Equation (1) to the temperature dependence of hydrodynamic diameter and the temperature dependence of the luminescence emitted by a single UCNP@PNIPAM.

	Min/nm	Max/nm	$T_{\text{tran}}/^\circ\text{C}$	$\tau/^\circ\text{C}$	R-square
Hydrodynamic diameter	$236 \pm 3$	$369 \pm 3$	$32.8 \pm 0.2$	$2.2 \pm 0.2$	0.992
Luminescence intensity	$0.92 \pm 0.04$	$1.65 \pm 0.02$	$32.0 \pm 0.5$	$2.3 \pm 0.5$	0.960

of the polymeric volume but also to an increase in its refractive index. The refractive index of PNIPAM at a temperature below VPTT can be approximated to 1.33,<sup>[21]</sup> comparable to that of water, when the PNIPAM is fully collapsed, its refractive index increases up to 1.47.<sup>[22]</sup> This change in refractive index follows a sigmoidal trend (Figure 1h).<sup>[23]</sup> The temperature-induced increment in the refractive index enhances the scattering efficiency of the UCNP@PNIPAM structures. This, in turn, causes an increment of the extinction (i.e., sum of scattering and absorption) coefficient of the colloidal dispersion of UCNP@PNIPAM structures as evidenced by optical transmission experiments (see Section S3 of the Supporting Information).

## 2.2. Optical Trapping of a Single UCNP@PNIPAM Structure

OT experiments were performed using a single beam optical trapping setup (in Figure 2a). When a single UCNP@PNIPAM structure gets trapped, the 980 nm laser radiation is partially absorbed by  $\text{Yb}^{3+}$  ions, which transfer their energy to nearby  $\text{Er}^{3+}$  ions, ultimately leading to strong red and green

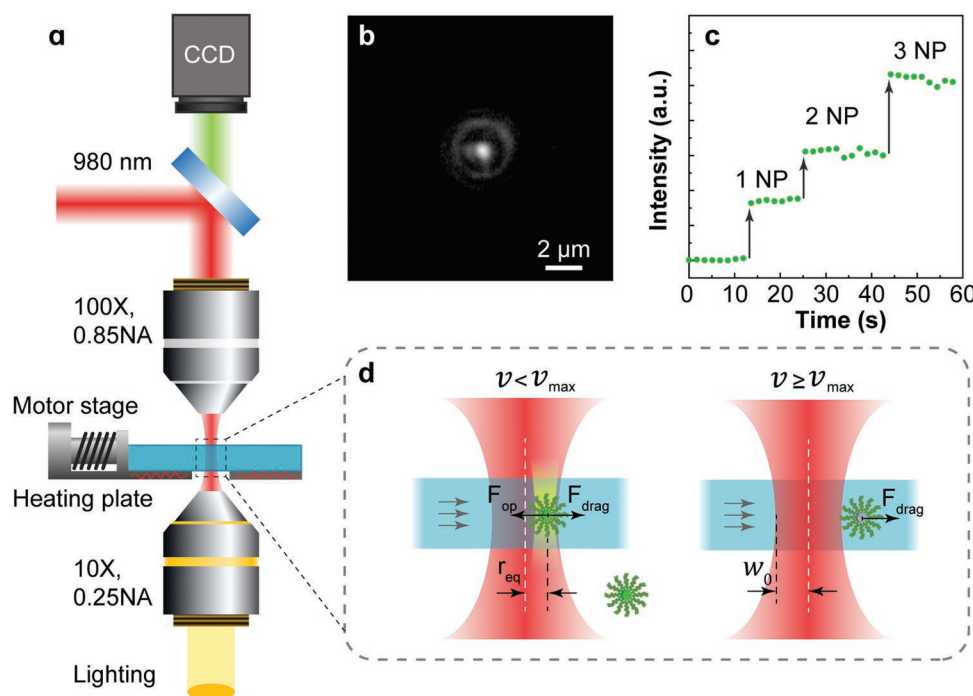


**Figure 2.** a) Experimental setup used for single-particle optical trapping experiments. b) Fluorescence image of a single optically trapped UCNP@PNIPAM at 20 °C. c) Luminescence intensity as a function of time obtained at 20 °C. Each step corresponds to a trapping event of a single UCNP@PNIPAM structure. d) Schematic drawings of the drag method used to measure the optical force.

emissions<sup>[24]</sup> (see Section S4 of the Supporting Information). The upconversion luminescence is collected by the same objective used for excitation and visualized by a charge-coupled device (CCD) camera. A condenser (10X, 0.25NA) is used to converge the white light from a light-emitting diode to get an optical image of the optical trap and surroundings in order to discard the presence of nanoparticle clusters. Figure 2b shows a fluorescence image of a single UCNP@PNIPAM structure optically trapped at room temperature. The incorporation of individual UCNP@PNIPAM structures into the trap was evidenced by discrete steps in the detected intensity (Figure 2c). The height of the intensity steps corresponds to the intensity of the emitted radiation generated by an individual UCNP@PNIPAM structure. The total luminescence intensity at the optical trap position allows determining the number of nanoparticles being optically trapped. It is worth noting that the optical trapping was performed 5  $\mu\text{m}$  above the bottom wall of the chamber. The local heating in the trap has been calculated to be below 3.63  $^{\circ}\text{C}$  (see the Supporting Information, Section S5).

The optical force that determines the trapping stability at different temperatures is calibrated by the drag method.<sup>[8b]</sup> As one can observe in Figure 2d, the motorized stage where the microchamber was placed allowed us to induce a relative velocity between the optically trapped UCNP and the surrounding medium. By recording the maximum velocity ( $v_{\text{max}}$ ) at which the sample stage can move to maintain the particle in the trap (see Section S6 of the Supporting Information), the maximum optical force ( $F_{\text{OT}}^{\text{max}} = \kappa w_0$ , being  $w_0$  the spot radius, i.e., the optical trap radius) is comparable to a drag force exerted on the trapped particle ( $F_{\text{drag}} = 6\pi\eta Rv_{\text{max}}$ , where  $R$  is the hydrodynamic radius of the trapped object and  $\eta$  is the dynamic viscosity of the medium (water in this case)). The power dependence of the maximum optical force at 20  $^{\circ}\text{C}$  was obtained for both bare UCNP and UCNP@PNIPAM structures (Figure 3a). In both cases,  $F_{\text{OT}}^{\text{max}}$  increases linearly with the laser power, being the optical force acting on the trapped UCNP enhanced by about 16 times thanks to the surface coating with PNIPAM. Such a staggering enhancement in the optical force ensures stable

optical trapping of a single UCNP@PNIPAM structure in high-viscosity media (such as cytoplasm of living cells) and above room temperature.<sup>[11a]</sup> Indeed, we have observed stable optical trapping of a single UCNP@PNIPAM structure for increasing temperatures up to 45  $^{\circ}\text{C}$  by using moderate/low laser powers (85 mW, Figure 3b). As the temperature rises, the trapping force acting on a single UCNP@PNIPAM structure decreases but remains larger than the one acting on a bare UCNP at room temperature.

Results reported in Figure 3 reveal how the PNIPAM coating improves both the strength and thermal stability of an optically trapped UCNP. The UCNP@PNIPAM structures show a diameter changing from 240 to 370 nm (Figure 1h). Within this size range, two formalisms may be applicable to describe optical forces: the Lorenz–Mie formalism (applied to particles whose size is comparable to the trapping wavelength) and the Rayleigh formalism (applied to particles with sizes much smaller than the trapping laser wavelength). The question here arising is which of these two formalisms better explains the results of Figure 3. Lorenz–Mie formalism states that optical forces scale with the size and the refractive index of the trapped particle.<sup>[25]</sup> Calculations included in Section S7 of the Supporting Information show that, in this Lorenz–Mie regime, the optical force should increase with temperature because the refractive index increment caused by the collapse of PNIPAM dominates over the size reduction. On the other hand, Rayleigh formalism states that optical forces should scale with the electronic polarizability of the trapped nanoparticle. Recent works demonstrate that the electronic polarizability of dielectric nanoparticles is mainly determined by their  $\zeta$ -potential and size.<sup>[9b]</sup> The collapse of the polymer does not affect the  $\zeta$ -potential of UCNP@PNIPAM structures (Section S2 of the Supporting Information). Thus, in a scenario of constant  $\zeta$ -potential, the electronic polarizability is expected to reduce with temperature due to the VPT of the PNIPAM that leads to a significant reduction of the UCNP@PNIPAM radius. Therefore, we conclude that Rayleigh formalism can explain the reduction of optical force with temperature experimentally observed (Figure 3b).

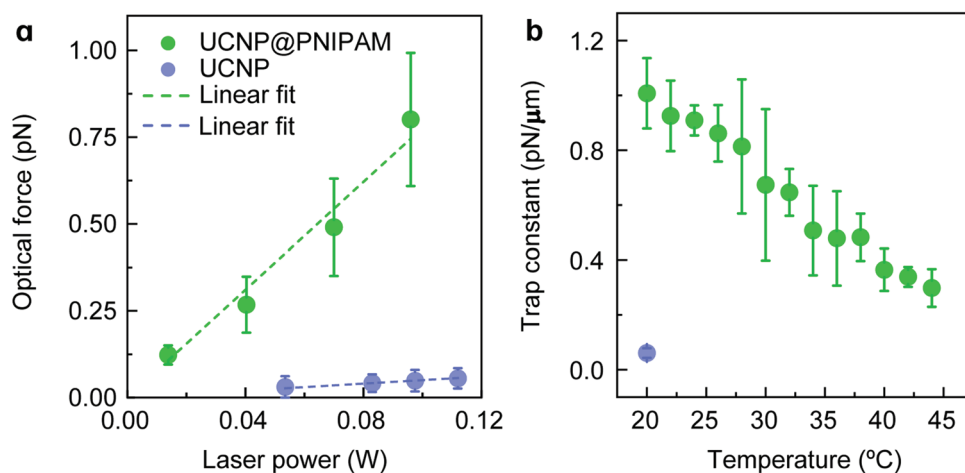


**Figure 3.** a) Comparison of optical forces acting on a single UCNP and a single UCNP@PNIPAM structure at 20  $^{\circ}\text{C}$ . b) Trapping constant of a single optically trapped UCNP@PNIPAM structure as a function of temperature, the laser power is 85 mW. At each temperature, at least four particles were measured, error comes from the standard deviation of multiple measurements.

### 2.3. Thermal Sensitivity of an Individual UCNP@PNIPAM Structure

After demonstrating that stable optical trapping of a single UCNP@PNIPAM structure over 40 °C is possible, its potential as a thermal nanosensor was assessed. The luminescence intensity generated by an optically trapped UCNP@PNIPAM structure as a function of temperature is shown in **Figure 4a** (see details in the Experimental Section). The error is estimated from the temporal fluctuations of luminescence intensity generated by a single trapped UCNP@PNIPAM structure at 20 °C<sup>[26]</sup> (**Figure 4b**). At low temperatures (20–25 °C), the luminescence intensity from a single UCNP@PNIPAM structure remains constant, then gradually increases with the increase of the temperature until 40 °C. Above 40 °C, the luminescence intensity tends to stabilize. The temperature evolution of the luminescence intensity can be fitted using the same four-parameter sigmoidal function that describes the PNIPAM collapse. The similar values found for the inflection point and half-width evidence the connection between the observed intensity increment and the collapse of the PNIPAM coating (**Table 1**). This causal link is further supported by the absence of any temperature-induced intensity increment in bare UCNP (see blue dots in **Figure 4a**). Furthermore, experimental data included in

Section S8 of the Supporting Information evidence that the intensity enhancement cannot be correlated with the incorporation of additional UCNP@PNIPAM structures into the trap. The physical mechanisms linking the PNIPAM collapse and the luminescence intensity enhancement are discussed in detail in the following section.

The relative thermal sensitivity ( $S_r(T)$ ) provided by the optically trapped UCNP@PNIPAM structure is defined as<sup>[26]</sup>

$$S_r(T) = \frac{1}{I_{UC}(T)} \frac{dI_{UC}(T)}{dT} \quad (2)$$

where  $I_{UC}(T)$  is the luminescence intensity at temperature  $T$ . **Figure 4c** reveals that the relative thermal sensitivity of an optically trapped UCNP@PNIPAM structure reaches 8% °C<sup>-1</sup> at 32 °C. This is significantly larger than the reported ratiometric relative thermal sensitivities of UCNP that are typically around 1% °C<sup>-1</sup> (see the comparison in Section S9 of the Supporting Information).<sup>[18–21]</sup> The temperature at which  $S_r(T)$  peaks well agree with the VPTT determined from the temperature dependence of hydrodynamic diameter reinforcing the connection between the temperature evolution of the luminescent properties of the UCNP@PNIPAM structure and the PNIPAM coating. Furthermore, in absence of the thermo-responsive

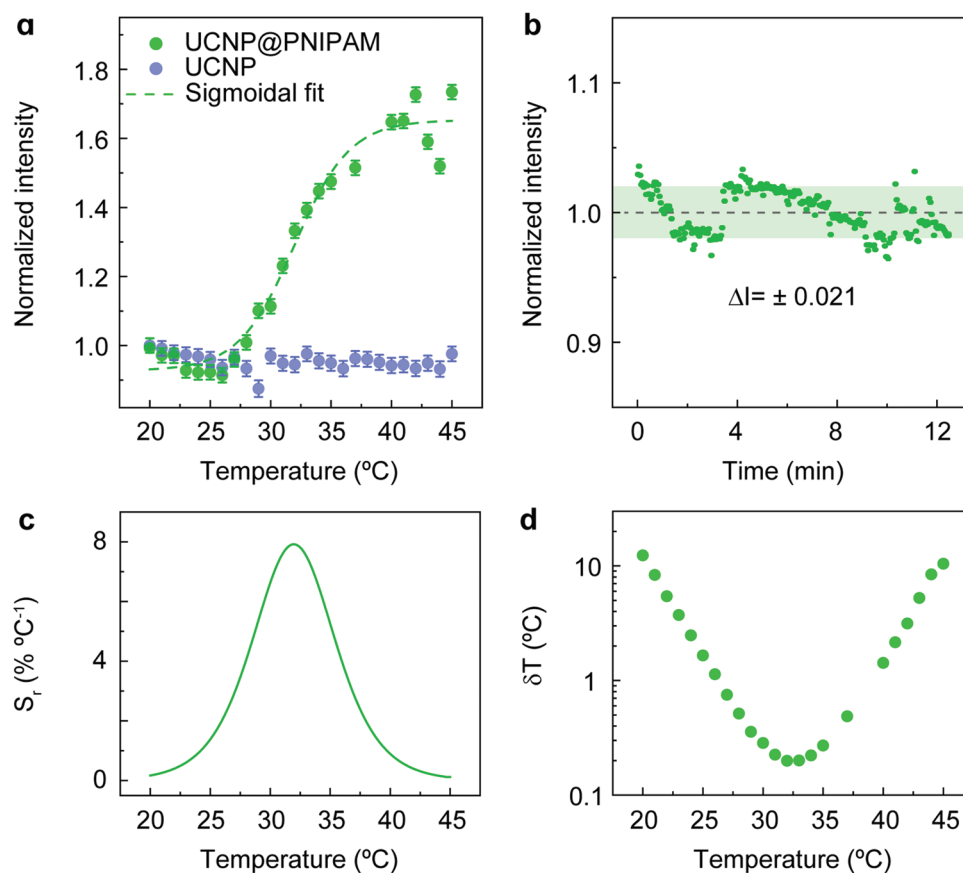


**Figure 4.** a) Temperature variation of luminescence intensity generated by a single UCNP or UCNPs@PNIPAM structure under the excitation and trapping of 980 nm laser, laser power is 85 mW. The error was estimated by the readout intensity fluctuation of a single UCNPs@PNIPAM at 20 °C in (b), where the intensity was normalized and the standard deviation was found to be  $\sigma = \Delta I = 0.021$ . c) Corresponding relative thermal sensitivities obtained from the sigmoidal fitting curve. d) Temperature uncertainty for temperature-dependent luminescence intensity of a single UCNPs@PNIPAM structure.

coating, the bare UCNP shows a negligible thermal sensitivity. The high thermal sensitivity achieved for temperatures close to VPTT leads to temperature uncertainties as low as 0.2 at 32 °C (Figure 4d), which has been calculated by<sup>[26]</sup>

$$\delta T = \frac{1}{S_r} \frac{\Delta I}{I} \quad (3)$$

In addition to the large thermal sensitivity and low temperature uncertainty, an extra advantage is that thermal sensing can be achieved directly from the analysis of emitted intensity without requiring any spectral analysis and, thus, simplifying the required experimental setup. As an evident drawback, the UCNP@PNIPAM structure shows an appreciable thermal sensitivity only in the surroundings of the VPTT so that they can be used only in those cases where the event to be monitored occurs in the temperature range corresponding to the polymer transition. However, tuning the operating temperature range can be easily achieved by tweaking the composition of the PNIPAM coating, theoretically leading to highly sensitive nanothermometers operating over a wide temperature range (10–55 °C).<sup>[27]</sup>

#### 2.4. Identification of the Mechanism behind the Large Thermal Sensitivity

Lastly, we investigated the cause of the PNIPAM-coating-induced increment in the luminescence intensity of a single UCNP@PNIPAM structure. Such increment should follow from an enhancement of the intrinsic emitted intensity by the UCNP or from an improvement in the excitation and/or emission collection efficiency. At a first glance, the most plausible explanation would be that the collapse of the PNIPAM coating expels the water molecules that are in contact with the UCNP surface. This, in turn, reduces the probability of nonradiative

decay events related to coupling with OH vibrations, which ultimately would lead to an increase in the radiative probability.<sup>[28]</sup> Thus, the removal of water molecules would cause an increment in the intensity emitted by the UCNP. If this was the case, a consequent lengthening of the fluorescence lifetime would be observed at increasing temperatures. A study of the fluorescence decay of Er<sup>3+</sup> emission as a function of temperature in UCNP@PNIPAM structures seems to rule out this hypothesis (Section S10 of the Supporting Information) since the fluorescence lifetime decreases monotonically with temperature.<sup>[29]</sup> The same trend was obtained for UCNP@PNIPAM structures in deuterated water and also when coating the UCNPs with a nonthermoresponsive polymer (see Section S10 of the Supporting Information). Therefore, it seems that the behavior of the de-excitation processes with temperature is not related to the collapse of the PNIPAM. Yet, because the fluorescence quantum yield of Er<sup>3+</sup> energy levels in UCNPs is generally characterized by low photoluminescence quantum yields,<sup>[30]</sup> the shape of the decay curves is expected to be dominated by nonradiative processes. Therefore, any change in the radiative decay that might occur could be difficult to appreciate from an inspection/analysis of the photoluminescence decay curves. This being said, we also moved to explore other sources of this unexpected increment in the intensity collected from the UCNP@PNIPAM structure: namely, possible improvements in the excitation and emission collection efficiency.

As discussed above, the PNIPAM shell collapse above the VPTT is accompanied by a refractive index increment. This change in refractive index transforms the PNIPAM coating into a high numerical aperture nanolens. The appearance of this PNIPAM nanolens simultaneously induces an extra focusing of laser (excitation) radiation and improves the collection efficiency of the luminescence.<sup>[11a,31]</sup> These two effects are schematically represented in Figure 5a. If we denote the excitation intensity amplification factor due to focusing by  $\beta_1 = I_{exc}^{int}/I_{exc}^{ext}$  (where  $I_{exc}^{int}$  and  $I_{exc}^{ext}$  are the 980 nm excitation intensity outside

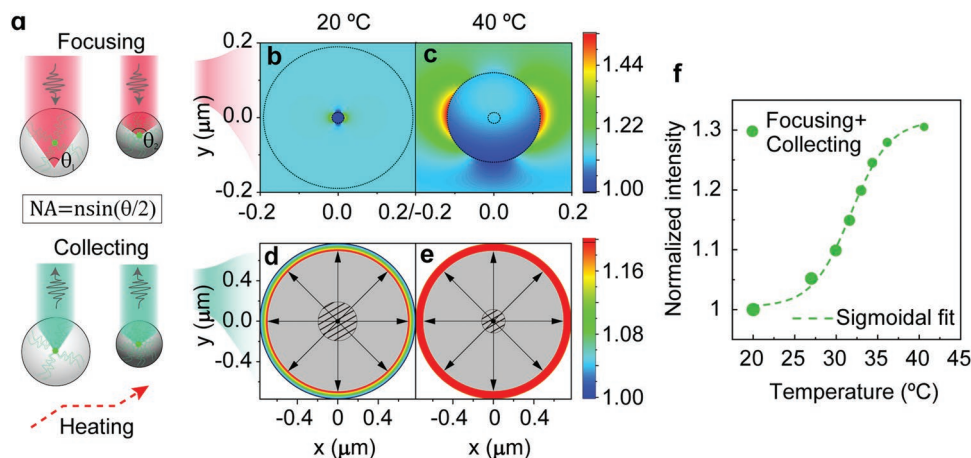


**Figure 5.** Nanolens effect simulations of PNIPAM coating. a) Schematic diagram: the polymer coating shrinks and its refractive index increases as temperature increases, resulting in the PNIPAM coating acting as a high numerical aperture nanolens with high focusing and collection efficiency at high temperatures. b,c) Two representative simulations of excitation intensity upon UCNP at 20 and 40 °C, corresponding to the focusing effect. d,e) Two representative simulations of emission intensity of UCNP at 20 and 40 °C, corresponding to the collecting effect. In both effects, the simulated intensity at 20 °C was set to 1 for ease of comparison at the center of the nanoparticle in (b) and at the boundary of the simulation box in (d). f) The calculated luminescence intensity of a single trapped UCNP@PNIPAM as a function of temperature considering lens effects generated by the PNIPAM coating (focusing and collecting effects).

and inside the UCNP core, respectively) and the collection efficiency by  $\beta_C$  (defined as the fraction of intensity generated by the UCNP core reaching the detector), then we can write the collected upconversion intensity,  $I_{UC}^c$ , as

$$I_{UC}^c = \beta_C \cdot (\beta_I \cdot I_{exc}^{ext})^n \quad (4)$$

where  $n$  is the order of the upconversion processes (number of infrared excitation photons required for the emission of a visible emitted photon). At the excitation intensity achieved within the optical trap ( $1500 \text{ kW cm}^{-2}$ ), we have experimentally verified that, due to saturation of intermediate states,<sup>[32]</sup> we are within the linear regime so that  $n = 1$  (see Section S11 in the Supporting Information). In these conditions, and considering that the laser excitation intensity was fixed during experiments (i.e.,  $I_{exc}^{ext}$  is constant and temperature-independent), we can state that the temperature-induced increase of the collected upconversion luminescence is given by the temperature dependence of both  $\beta_I$  and  $\beta_C$  in such a way that

$$I_{UC}^c(T) = \beta_C(T) \cdot \beta_I(T) \cdot I_{exc}^{ext} \quad (5)$$

Numerical simulations have been performed to obtain the temperature-induced variation of both  $\beta_I$  and  $\beta_C$ .

We have first considered a single UCNP@PNIPAM structure within a collimated 980 nm laser beam and numerical calculations were performed to determine the intensity of 980 nm radiation within the UCNP core.<sup>[33]</sup> Due to the small size of the UCNP core compared to the overall UCNP@PNIPAM structure, the system is here described as a solid sphere filled with the PNIPAM polymer. Numerical simulations, based on the Mie scattering equation for a coated sphere, have shown how the creation of a high numerical aperture PNIPAM nanolens refocuses the trapping laser and causes an increment of the excitation laser intensity within the UCNP core. Figure 5b shows the calculated 980 laser intensity within an UCNP@PNIPAM structure at 20 °C. At this temperature, the refractive index of the PNIPAM coating (indicated by the blue dots in Figure 1h) is very close to that of water and, therefore, it does not contribute to any laser refocusing. At 40 °C, after the PNIPAM volume contraction and refractive index increment, the calculations anticipate a relevant increment (12%, see Section S12 in the Supporting Information) in the 980 nm laser excitation intensity within the UCNP (Figure 5c). The magnitude of this increment depends on the temperature since it is a function of the temperature-induced variation of the refractive index, following a four-parameter sigmoidal function (as discussed in Section S12 of the Supporting Information). Notably, artificial focusing of excitation radiation at the microscale has already been proven an efficient way of improving the luminescence intensity generated by UCNPs.<sup>[11a,31]</sup>

The creation of a PNIPAM nanolens also impacts the luminescence collection efficiency by inducing an additional refocusing of the emitted radiation. To estimate the magnitude of the enhancement in the intensity of collected luminescence, we performed numerical simulations in which the UCNP@PNIPAM structure is considered as a radiative dipole (centered at the UCNP core and polarized in the Z-direction)

surrounded by a shell of variable thickness and refractive index depending on temperature. Figure 5d,e shows the 2D spatial variation of the emitted (radiated) intensity as obtained below and above the VPTT. The color map represents the value of the intensity in a space region defined as a circular corona around the dipole. The striped circle represents the PNIPAM and the arrows represent the direction of the emission from the dipole. Figure 5d corresponds to  $T = 20 \text{ °C}$  while Figure 5e is for  $T = 40 \text{ °C}$ . For ease of comparison, the intensity for  $T = 20 \text{ °C}$  at the boundaries of the simulation box ( $0.8 \text{ }\mu\text{m}$  from the center) has been set to unity (blue in the color bar). Note how for  $T = 40 \text{ °C}$  (Figure 5e), the intensity at the same distance from the center increases by a factor of 1.17 (dark orange in the color bar). From these results, it is evident how the collapse of the PNIPAM shell leads to a marked (17%) enhancement in the UCNP radiated intensity. More details about these calculations can be found in Section S12 of the Supporting Information where, again, it is shown that this enhancement follows a four-parameter sigmoidal function with temperature. These simulations were performed using finite element methods.

Thus, numerical calculations reveal that both  $\beta_C(T)$  and  $\beta_I(T)$  increase with the temperature due to the collapse of the PNIPAM shell. Figure 5f shows the temperature variation of the product  $\beta_C(T) \cdot \beta_I(T)$ . Numerical calculations, therefore, predict a temperature-induced increment of the collected luminescence intensity close to 30%. This numerical prediction is smaller but of the same order of magnitude as the intensity enhancement experimentally obtained (close to 65% as shown in Figure 4a). Discrepancies between numerical simulations and experimental data could be explained by considering changes in the position of the UCNP@PNIPAM structure within the trap (leading to different excitation intensities) or to an underestimation of the temperature-induced increment in the local refractive index of PNIPAM coating. As mentioned above, the temperature-induced enhancement in the collected visible luminescence could also be partially caused by an increment in the radiative probability of erbium ions due to the increment in the local refractive index.<sup>[34]</sup> Due to the low quantum yield of Erbium emission, this change in radiative lifetime would not be detected by lifetime measurements but could be contributing to the experimentally observed increment in the intensity of visible luminescence. Despite this discrepancy, the comparable trend of numerical simulations and experimental data reveals that the observed increment in the emitted intensity of an optically trapped UCNP@PNIPAM structure is mostly caused by the changes induced in the PNIPAM coating. Of course, the magnitude of the emission enhancement would depend on the thickness of the PNIPAM coating, and it could vary between nanoparticles although variation is expected to be small thanks to the narrow size dispersion observed in DLS measurements as discussed above (see Figure 1h).

### 3. Conclusions

We provided a blueprint for the preparation of highly sensitive luminescent nanothermometers based on the combination of UCNPs and a thermoresponsive polymer PNIPAM.



Specifically, PNIPAM acts simultaneously at several levels, making the UCNP@PNIPAM structure a far superior thermal nanosensor at the single-particle level compared to an uncoated UCNP. First, the presence of the polymeric coating leads to a >10-fold increment in the optical force, enabling stable trapping above room temperature (up to 45 °C) and, foreseeably, in viscous media. Second, the collapse of the PNIPAM coating induces an anomalous temperature dependence of the luminescence intensity generated by the optically trapped UCNP@PNIPAM structure, ultimately translating to maximum sensitivities around the transition temperature of the thermoresponsive polymer well above the ones classically reported for Yb<sup>3+</sup>, Er<sup>3+</sup>-doped UCNPs (8% vs ≈1% °C<sup>-1</sup>). Numerical simulations revealed that this temperature-induced enhancement in the emitted intensity can be explained regarding the PNIPAM coating as a high numerical aperture nanolens. Such nanolens increases the excitation intensity within the UCNP while also improving the fluorescence collection efficiency.

This work reveals how a rational surface functionalization can expand the potential application of upconverting nanoparticles. Note that these results were demonstrated as a proof-of-concept for a single PNIPAM coating. However, the transition temperature of this thermoresponsive polymer can be modified ad hoc upon tailoring its composition and polymerization degree, thus preparing nanothermometer with a customizable working range. In particular, the nanoparticles here developed can be used in high-sensitivity and high-spatial-resolution 3D thermal imaging by using a single optically controlled UCNP. This opens the possibility of, e.g., achieving thermal images of living cells by particle scanning within the cytoplasm or exploring thermal gradients in the sub-micrometric scale created within microfluidic devices.

## 4. Experimental Section

**Single-Particle Trapping:** Using a high-numerical-aperture (Olympus, LCPLN 100x IR, 0.85 NA) microscope objective, a 980 nm laser beam generated by a single-mode fiber-coupled diode was focused into the microchamber containing the dilute aqueous dispersion of UCNP@PNIPAM structures. The spot radius  $w_0$  of the laser was calculated to be 700 nm. A 120 μm high microchamber, which was formed by pasting a Secure Seal spacer on a microscope slide, was attached to a heating plate (model T95-PE, Linkam Scientific Instruments Ltd.) mounted on a motorized sample stage. This set-up afforded a fine temperature control over the trap volume with the thermal stability of 0.1 °C and relative motion between the trapped particle and the surrounding medium. In practice, the UCNP@PNIPAM structures tended to adsorb on the surface of the negatively charged glass slide. In order to avoid adhesion, the glass slide surface was preemptively treated with polyethylenimine (PEI) to minimize electrostatic interactions (see details in Section S1.4 of the Supporting Information). By adjusting the concentration of the colloidal dispersion of UCNP@PNIPAM and the trapping power, the loading rate of UCNP@PNIPAM at the trap position could be controlled. In Figure 2c, the concentration of UCNP@PNIPAM structures aqueous solution was set to be 10<sup>9</sup> UCNP@PNIPAM structures mL<sup>-1</sup> and the on-target trapping power was 85 W. For single-particle trapping experiments, the aqueous dispersion of UCNP@PNIPAM structures was further diluted to 3 × 10<sup>6</sup> UCNP@PNIPAM mL<sup>-1</sup> corresponding to an interparticle average distance of 70 μm. Such a low concentration was required to avoid multiple-particle trapping. Before measurement, the dispersion was sonicated for 30 min to eliminate possible particle aggregates.

**Drag Method:** The experimental set-up used in this work allowed to induce a relative velocity between the optically trapped UCNP and the surrounding medium by translating the motorized sample stage. Once a relative velocity  $v$  was induced, a drag force appeared:  $F_{\text{drag}} = 6\pi\eta Rv$ , where  $R$  is the hydrodynamic radius of the trapped object and  $\eta$  is the dynamic viscosity of the medium (water in this case). As can be observed in Figure 2d, this drag force displaced a trapped particle away from its equilibrium position by a distance  $r_{\text{eq}}$ . To balance the drag force, an optical force with a restoring nature appeared, whose magnitude was  $F_{\text{OT}} = \kappa r_{\text{eq}}$ , where the trap constant ( $\kappa$ ) is, in a first-order approximation, proportional to the laser power. When the drag force overcame the maximum optical force ( $F_{\text{OT}}^{\text{max}} = \kappa w_0$ , being  $w_0$  the spot radius, i.e., the optical trap radius), the UCNP@PNIPAM structure escaped from the trap. This occurred when the relative velocity reached the maximum velocity,  $v_{\text{max}}$ , given by:  $F_{\text{OT}}^{\text{max}} = 6\pi\eta Rv_{\text{max}} = \kappa w_0$ . Thus, experimental determination of  $v_{\text{max}}$  allowed finding the maximum optical force.

**Emission Intensity Measurement:** The luminescence intensity generated by a single UCNP or UCNP@PNIPAM under the excitation and trapping of 980 nm laser at different temperatures was obtained by processing the fluorescence images taken by CCD camera (QImaging QIClick Camera, Model: QIClick-F-M-12, monochrome, 12-bit). First, put microchamber on sample stage, then set temperature of the heating plate at 20 °C. Turned on the laser, make sure the laser power was around 85 mW, and waited for the particle getting into the trap. Once a single particle was trapped at 20 °C, the temperature in the trap volume was increased at a 2 °C min<sup>-1</sup> rate, simultaneously recording fluorescence images of the trapped particle with an exposure time of 3 s. Maintaining the temperature of the heating plate at 20 °C, fluctuations of luminescence intensity generated by a single trapped UCNP@PNIPAM at 20 °C were measured with the same exposure time of 3 s.

**Statistical Analysis:** The measurements of temperature-dependent  $\zeta$ -potential and hydrodynamic size were performed using the same UCNP@PNIPAM dispersion. The presented data in Figure 1h and Figure S3b in the Supporting Information were obtained as an average of three consecutive measurements and errors represented the standard deviation.

The optical force measurement of a single particle was performed at least four particles. The data presented in Figure 3 were an average of multiple measurements and the error bar was the standard deviation.

For the detection of emission intensity with a CCD camera (see Figure 4a), the intensity at different temperatures was obtained by processing the fluorescence images. The error was estimated by the readout intensity fluctuation of a single UCNP@PNIPAM trapped by the same laser with the same power at 20 °C. Indeed, the effect of temperature on intensity fluctuations was not considered here.

## Supporting Information

Supporting Information is available from the Wiley Online Library or from the author.

## Acknowledgements

This work was supported by the Ministerio de Ciencia e Innovación de España (PID2019-106211RB-I00 PID2019-105195RA-I00 and MAT2017-83111R), by the Comunidad de Madrid (S2017/BMD-3867 RENIM-CM), co-financed by European Structural and Investment Fund and by the Universidad Autónoma de Madrid and Comunidad Autónoma de Madrid (SI1/PJ1/2019-00052 and PR38/21-36 ANTICIPA-CM). D.L. acknowledges a scholarship from the China Scholarship Council (201808350097). J.R.B. acknowledges the support from Carl Tryggers Foundation (CTS18:229). M.I.M. acknowledges financial support from the Spanish Ministerio de Ciencia e Innovación, through the “María de Maeztu” Programme for Units of Excellence in R&D (CEX2018-000805-M) and the MELODIA PGC2018-095777-B-C22 project.

## Conflict of Interest

The authors declare no conflict of interest.

## Data Availability Statement

The data that support the findings of this study are available from the corresponding author upon reasonable request.

## Keywords

luminescent nanothermometry, optical force, optical trapping, poly(*N*-isopropylacrylamide), surface modification, thermal sensitivity, upconverting nanoparticles

Received: April 19, 2022  
Revised: June 29, 2022  
Published online: July 30, 2022

- [1] a) D. Jaque, F. Vetrone, *Nanoscale* **2012**, *4*, 4301; b) C. D. Brites, P. P. Lima, N. J. Silva, A. Millan, V. S. Amaral, F. Palacio, L. D. Carlos, *Nanoscale* **2012**, *4*, 4799; c) B. del Rosal, E. Ximendes, U. Rocha, D. Jaque, *Adv. Opt. Mater.* **2017**, *5*, 1600508; d) H. Zhao, A. Vomiero, F. Rosei, *Small* **2015**, *11*, 5741; e) A. Bednarkiewicz, L. Marciniak, L. D. Carlos, D. Jaque, *Nanoscale* **2020**, *12*, 14405; f) F. Vetrone, R. Naccache, A. Zamarrón, A. Juarranz de la Fuente, F. Sanz-Rodríguez, L. Martínez Maestro, E. Martín Rodríguez, D. Jaque, J. García Sole, J. A. Capobianco, *ACS Nano* **2010**, *4*, 3254.
- [2] a) B. Zhou, B. Shi, D. Jin, X. Liu, *Nat. Nanotechnol.* **2015**, *10*, 924; b) M. Quintanilla, L. M. Liz-Marzan, *Nano Today* **2018**, *19*, 126; c) E. Hemmer, P. Acosta-Mora, J. Mendez-Ramos, S. Fischer, *J. Mater. Chem. B* **2017**, *5*, 4365; d) H. Dong, S.-R. Du, X.-Y. Zheng, G.-M. Lyu, L.-D. Sun, L.-D. Li, P.-Z. Zhang, C. Zhang, C.-H. Yan, *Chem. Rev.* **2015**, *115*, 10725; e) E. M. Chan, *Chem. Soc. Rev.* **2015**, *44*, 1653; f) X. Wu, Y. Zhang, K. Takle, O. Bilsel, Z. Li, H. Lee, Z. Zhang, D. Li, W. Fan, C. Duan, *ACS Nano* **2016**, *10*, 1060; g) F. Wang, D. Banerjee, Y. Liu, X. Chen, X. Liu, *Analyst* **2010**, *135*, 1839; h) C. Lee, E. Z. Xu, Y. Liu, A. Teitelboim, K. Yao, A. Fernandez-Bravo, A. M. Kotulska, S. H. Nam, Y. D. Suh, A. Bednarkiewicz, *Nature* **2021**, *589*, 230.
- [3] a) C. Xu, Y. Huang, Y. Lin, J. Huang, X. Gong, Z. Luo, Y. Chen, *Opt. Lett.* **2017**, *42*, 3383; b) M. Jia, G. Liu, Z. Sun, Z. Fu, W. Xu, *Inorg. Chem.* **2018**, *57*, 1213; c) H. Suo, C. Guo, J. Zheng, B. Zhou, C. Ma, X. Zhao, T. Li, P. Guo, E. M. Goldys, *ACS Appl. Mater. Interfaces* **2016**, *8*, 30312.
- [4] a) X. Zhu, J. Li, X. Qiu, Y. Liu, W. Feng, F. Li, *Nat. Commun.* **2018**, *9*, 2176; b) X. Zhu, W. Feng, J. Chang, Y.-W. Tan, J. Li, M. Chen, Y. Sun, F. Li, *Nat. Commun.* **2016**, *7*, 10437; c) A. R. Bastos, C. D. Brites, P. A. Rojas-Gutierrez, C. DeWolf, R. A. Ferreira, J. A. Capobianco, L. D. Carlos, *Adv. Funct. Mater.* **2019**, *29*, 1905474; d) J. Zhou, B. Del Rosal, D. Jaque, S. Uchiyama, D. Jin, *Nat. Methods* **2020**, *17*, 967.
- [5] a) X. Qiu, Q. Zhou, X. Zhu, Z. Wu, W. Feng, F. Li, *Nat. Commun.* **2020**, *11*, 4; b) D. H. Ortgies, M. Tan, E. C. Ximendes, B. Del Rosal, J. Hu, L. Xu, X. Wang, E. Martín Rodríguez, C. Jacinto, N. Fernandez, *ACS Nano* **2018**, *12*, 4362; c) E. S. Levy, C. A. Tajon, T. S. Bischof, J. Iafrazi, A. Fernandez-Bravo, D. J. Garfield, M. Chamanzar, M. M. Maharbiz, V. S. Sohal, P. J. Schuck, *ACS Nano* **2016**, *10*, 8423.
- [6] a) M. A. Gatoó, S. Naseem, M. Y. Arfat, A. Mahmood Dar, K. Qasim, S. Zubair, *Biomed. Res. Int.* **2014**, *2014*, 498420; b) A. Gnach, T. Lipinski, A. Bednarkiewicz, J. Rybka, J. A. Capobianco, *Chem. Soc. Rev.* **2015**, *44*, 1561.
- [7] a) E.-L. Florin, A. Pralle, *J. Struct. Biol.* **1997**, *119*, 202; b) Y. Zhang, W. Zhu, F. Hui, M. Lanza, T. Borca-Tasciuc, M. M. Rojo, *Adv. Funct. Mater.* **2020**, *30*, 1900892.
- [8] a) P. Rodríguez-Sevilla, H. Rodríguez-Rodríguez, M. Pedroni, A. Speghini, M. Bettinelli, J. G. Solé, D. Jaque, P. Haro-González, *Nano Lett.* **2015**, *15*, 5068; b) P. Rodríguez-Sevilla, L. Labrador-Páez, D. Jaque, P. Haro-González, *J. Mater. Chem. B* **2017**, *5*, 9085; c) P. Rodríguez-Sevilla, L. Labrador-Páez, D. Wawrzyńczyk, M. Nyk, M. Samoć, A. K. Kar, M. D. Mackenzie, L. Paterson, D. Jaque, P. Haro-González, *Nanoscale* **2016**, *8*, 300; d) P. Rodríguez-Sevilla, Y. Zhang, N. de Sousa, M. I. Marqués, F. Sanz-Rodríguez, D. Jaque, X. Liu, P. Haro-González, *Nano Lett.* **2016**, *16*, 8005; e) P. Rodríguez-Sevilla, Y. Arita, X. Liu, D. Jaque, K. Dholakia, *ACS Photonics* **2018**, *5*, 3772; f) P. Rodríguez-Sevilla, T. Lee, L. Liang, P. Haro-González, G. Lifante, X. Liu, D. Jaque, *Adv. Opt. Mater.* **2018**, *6*, 1800161; g) E. Ortiz-Rivero, K. Prorok, M. Skowicki, D. Lu, A. Bednarkiewicz, D. Jaque, P. Haro-González, *Small* **2019**, *15*, 1904154; h) D. Lu, L. Labrador-Páez, E. Ortiz-Rivero, P. Frades, M. A. Antoniak, D. Wawrzyńczyk, M. Nyk, C. D. Brites, L. D. Carlos, J. A. García Solé, *Nano Lett.* **2020**, *20*, 8024; i) N. Panov, D. Lu, E. Ortiz-Rivero, E. Martinazzo Rodrigues, P. Haro-González, D. Jaque, E. Hemmer, *Adv. Opt. Mater.* **2021**, *9*, 2100101; j) K. Dholakia, P. Reece, M. Gu, *Chem. Soc. Rev.* **2008**, *37*, 42; k) M. Gu, S. Kuriakose, X. Gan, *Opt. Express* **2007**, *15*, 1369.
- [9] a) D. Gao, W. Ding, M. Nieto-Vesperinas, X. Ding, M. Rahman, T. Zhang, C. Lim, C.-W. Qiu, *Light: Sci. Appl.* **2017**, *6*, e17039; b) P. Rodríguez-Sevilla, K. Prorok, A. Bednarkiewicz, M. I. Marqués, A. García-Martín, J. García Solé, P. Haro-González, D. Jaque, *Nano Lett.* **2018**, *18*, 602.
- [10] P. Rodríguez-Sevilla, Y. Zhang, P. Haro-Gonzalez, F. Sanz-Rodríguez, F. Jaque, J. G. Sole, X. Liu, D. Jaque, *Adv. Mater.* **2016**, *28*, 2421.
- [11] a) D. Lu, M. Pedroni, L. Labrador-Páez, M. I. Marqués, D. Jaque, P. Haro-González, *Small* **2021**, *17*, 2006764; b) O. M. Maragó, P. H. Jones, P. G. Gucciardi, G. Volpe, A. C. Ferrari, *Nat. Nanotechnol.* **2013**, *8*, 807; c) S. Kawata, Y. Inouye, P. Verma, *Nat. Photonics* **2009**, *3*, 388; d) P. Kang, X. Serey, Y.-F. Chen, D. Erickson, *Nano Lett.* **2012**, *12*, 6400.
- [12] a) T. Davis, *Opt. Express* **2007**, *15*, 2702; b) D. Lu, F. Gámez, P. Haro-González, *Micromachines* **2021**, *12*, 954.
- [13] a) H. Rodríguez-Rodríguez, P. R. Sevilla, E. M. Rodriguez, D. H. Ortgies, M. Pedroni, A. Speghini, M. Bettinelli, D. Jaque, P. Haro-González, *Small* **2015**, *11*, 1555; b) M. Wang, G. Abbineni, A. Clevenger, C. Mao, S. Xu, *Nanomed.: Nanotechnol., Biol. Med.* **2011**, *7*, 710.
- [14] a) Y. H. Lin, M. E. McConney, M. C. LeMieux, S. Peleshanko, C. Jiang, S. Singamaneni, V. V. Tsukruk, *Adv. Mater.* **2006**, *18*, 1157; b) C.-M. Yang, W.-Y. Zeng, Y.-P. Chen, *IEEE Sens. J.* **2018**, *18*, 2253; c) A. Sedlmeier, H. H. Gorris, *Chem. Soc. Rev.* **2015**, *44*, 1526; d) V. Muhr, S. Wilhelm, T. Hirsch, O. S. Wolfbeis, *Acc. Chem. Res.* **2014**, *47*, 3481; e) G.-S. Yi, G.-M. Chow, *Chem. Mater.* **2007**, *19*, 341; f) L. Labrador-Páez, E. C. Ximendes, P. Rodríguez-Sevilla, D. H. Ortgies, U. Rocha, C. Jacinto, E. M. Rodríguez, P. Haro-González, D. Jaque, *Nanoscale* **2018**, *10*, 12935; g) F. Vetrone, R. Naccache, V. Mahalingam, C. G. Morgan, J. A. Capobianco, *Adv. Funct. Mater.* **2009**, *19*, 2924.
- [15] a) K. Fujimoto, Y. Nakajima, M. Kashiwabara, H. Kawaguchi, *Polym. Int.* **1993**, *30*, 237; b) M. Wei, M. J. Serpe, *Part. Part. Syst. Charact.* **2019**, *36*, 1800326; c) M. Agrawal, J. Rubio-Retama, N. Zafeiropoulos, N. Gaponik, S. Gupta, V. Cimrova, V. Lesnyak, E. López-Cabarcos, S. Tzavalas, R. Rojas-Reyna, *Langmuir* **2008**, *24*, 9820; d) Q. Xiao, Y. Li, F. Li, M. Zhang, Z. Zhang, H. Lin, *Nanoscale* **2014**, *6*, 10179.
- [16] a) J. Rubio Retama, B. Frick, T. Seydel, M. Stamm, A. Fernandez Barbero, E. Lopez Cabarcos, *Macromolecules* **2008**, *41*, 4739;

- b) B. Sierra-Martin, J. R. Retama, M. Laurenti, A. F. Barbero, E. L. Cabarcos, *Adv. Colloid Interface Sci.* **2014**, 205, 113; c) Y. Guan, Y. Zhang, *Soft Matter* **2011**, 7, 6375; d) F. Doberenz, K. Zeng, C. Willems, K. Zhang, T. Groth, *J. Mater. Chem. B* **2020**, 8, 607.
- [17] J.-C. Boyer, F. Vetrone, L. A. Cuccia, J. A. Capobianco, *J. Am. Chem. Soc.* **2006**, 128, 7444.
- [18] A. Fernández-Barbero, I. J. Suárez, B. Sierra-Martín, A. Fernández-Nieves, F. J. de Las Nieves, M. Marquez, J. Rubio-Retama, E. López-Cabarcos, *Adv. Colloid Interface Sci.* **2009**, 147, 88.
- [19] S. Hirotsu, I. Yamamoto, A. Matsuo, T. Okajima, H. Furukawa, T. Yamamoto, *J. Phys. Soc. Jpn.* **1995**, 64, 2898.
- [20] S. Hormeño, P. Gregorio-Godoy, J. Pérez-Juste, L. M. Liz-Marzán, B. H. Juárez, J. R. Arias-Gonzalez, *Small* **2014**, 10, 376.
- [21] B. W. Garner, Z. Hu, F. D. McDaniel, A. Neogi, *MRS Online Proc. Libr.* **2007**, 1060, 608.
- [22] M. Philipp, U. Müller, R. Aleksandrova, R. Sanctuary, P. Müller-Buschbaum, J. K. Krüger, *Soft Matter* **2012**, 8, 11387.
- [23] M. E. Harmon, D. Kuckling, C. W. Frank, *Macromolecules* **2003**, 36, 162.
- [24] D. J. Gargas, E. M. Chan, A. D. Ostrowski, S. Aloni, M. V. P. Altoe, E. S. Barnard, B. Sanii, J. J. Urban, D. J. Milliron, B. E. Cohen, *Nat. Nanotechnol.* **2014**, 9, 300.
- [25] a) T. A. Nieminen, V. L. Loke, A. B. Stilgoe, G. Knöner, A. M. Brańczyk, N. R. Heckenberg, H. Rubinsztein-Dunlop, *J. Opt. A: Pure Appl. Opt.* **2007**, 9, S196; b) D. K. Gupta, D. Karthickeyan, B. Tata, T. Ravindran, *Colloid Polym. Sci.* **2016**, 294, 1901.
- [26] C. Brites, A. Millán, L. Carlos, in *Handbook on the Physics and Chemistry of Rare Earths*, Vol. 49 (Ed: J.-C. Bünzli, V. K. Pecharsky), Elsevier, New York **2016**, pp. 339.
- [27] a) S. Chen, K. Wang, W. Zhang, *Polym. Chem.* **2017**, 8, 3090; b) D. Crespy, R. M. Rossi, *Polym. Int.* **2007**, 56, 1461.
- [28] F. T. Rabouw, P. T. Prins, P. Villanueva-Delgado, M. Castelijns, R. G. Geitenbeek, A. Meijerink, *ACS Nano* **2018**, 12, 4812.
- [29] X. Liu, A. Skripka, Y. Lai, C. Jiang, J. Liu, F. Vetrone, J. Liang, *Nat. Commun.* **2021**, 12, 6401.
- [30] a) M. D. Wisser, S. Fischer, C. Siefe, A. P. Alivisatos, A. Salleo, J. A. Dionne, *Nano Lett.* **2018**, 18, 2689; b) S. Balabhadra, M. Debasu, C. Brites, R. Ferreira, L. Carlos, *J. Lumin.* **2017**, 189, 64.
- [31] a) L. Dong, A. K. Agarwal, D. J. Beebe, H. Jiang, *Nature* **2006**, 442, 551; b) Q. Liu, H. Liu, D. Li, W. Qiao, G. Chen, H. Ågren, *Nanoscale* **2019**, 11, 14070; c) X. Chen, T. Wu, Z. Gong, J. Guo, X. Liu, Y. Zhang, Y. Li, P. Ferraro, B. Li, *Light: Sci. Appl.* **2021**, 10, 242.
- [32] M. Pollnau, D. R. Gamelin, S. Lüthi, H. Güdel, M. P. Hehlen, *Phys. Rev. B* **2000**, 61, 3337.
- [33] H. Suzuki, S. I-Yin, *Int. J. Phys. Sci.* **2008**, 3, 38.
- [34] R. Meltzer, W. Yen, H. Zheng, S. Feofilov, M. Dejneka, B. Tissue, H. Yuan, *J. Lumin.* **2001**, 94, 217.